

DENSE MOLECULAR GAS AND THE ROLE OF STAR FORMATION¹ IN THE HOST GALAXIES OF QUASI-STELLAR OBJECTS

A. S. EVANS,¹ P. M. SOLOMON,¹ L. J. TACCONI,² T. VAVILKIN,¹ AND D. DOWNES³

Received 2006 July 1; accepted 2006 August 14

ABSTRACT

New millimeter-wave CO and HCN observations of the host galaxies of infrared-excess Palomar-Green (PG) quasi-stellar objects (QSOs) previously detected in CO are presented. These observations are designed to assess the validity of using the infrared luminosity to estimate star formation rates of luminous active galactic nuclei (AGNs) by determining the relative significance of dust heating by young, massive stars and AGNs in QSO hosts and *IRAS* galaxies with warm, AGN-like infrared colors. The analysis of these data is based, in part, on evidence that HCN traces high-density ($>10^4 \text{ cm}^{-3}$) molecular gas, and that the starburst-to-HCN luminosity ratio, $L_{\text{SB}}/L'_{\text{HCN}}$, of *IRAS*-detected galaxies is constant. The new CO data provide a confirmation of prior claims that PG QSO hosts have high infrared-to-CO luminosity ratios, $L_{\text{IR}}/L'_{\text{CO}}$, relative to *IRAS* galaxies of comparable L_{IR} . Such high $L_{\text{IR}}/L'_{\text{CO}}$ ratios may be due to significant heating of dust by the QSO or to an increased star formation efficiency in QSO hosts relative to the bulk of the luminous *IRAS* galaxy population. The HCN data show a similar trend, with the PG QSO host I Zw 1 and most of the warm *IRAS* galaxies having high $L_{\text{IR}}/L'_{\text{HCN}}$ (>1600) relative to the cool *IRAS* galaxy population, for which the median $\langle L_{\text{IR}}/L'_{\text{HCN}} \rangle_{\text{cool}} \sim 890^{+440}_{-470}$. If the assumption is made that the infrared emission from cool *IRAS* galaxies is reprocessed light from embedded star-forming regions, then high values of $L_{\text{IR}}/L'_{\text{HCN}}$ are likely the result of dust heating by the AGNs. Further, if the median ratio of $L'_{\text{HCN}}/L'_{\text{CO}} \sim 0.06$ observed for Seyfert galaxies and I Zw 1 is applied to the PG QSOs not detected in HCN, then the derived $L_{\text{IR}}/L'_{\text{HCN}}$ values correspond to a stellar contribution to the production of L_{IR} of $\sim 7\%–39\%$, and star formation rates of $\sim 2–37 M_{\odot} \text{ yr}^{-1}$ are derived for the QSO hosts. The corresponding values for the warm galaxies are $\sim 10\%–100\%$ and $\sim 3–220 M_{\odot} \text{ yr}^{-1}$. Alternatively, if the far-infrared is adopted as the star formation component of the total infrared in cool galaxies, i.e., $\langle L_{\text{FIR}}/L'_{\text{HCN}} \rangle_{\text{cool}} \sim L_{\text{SB}}/L'_{\text{HCN}}$, the stellar contributions in QSO hosts and warm galaxies to their L_{FIR} are up to 35% and 10% higher, respectively, than the percentages derived for L_{IR} . This raises the possibility that the L_{FIR} in several of the PG QSO hosts, including I Zw 1, could be due entirely to dust heated by young, massive stars. Finally, there is no evidence that the global HCN emission is enhanced relative to CO in galaxies hosting luminous AGNs.

Key words: galaxies: active — galaxies: interactions — galaxies: ISM — infrared: galaxies — ISM: molecules — quasars: general

1. INTRODUCTION

Over the last two decades, considerable progress has been made in investigating the possible evolutionary connection between ultraluminous infrared galaxy (ULIG, i.e., $L_{\text{IR}}[8–1000 \mu\text{m}] \geq 10^{12} L_{\odot}$) mergers and quasi-stellar objects (QSOs) first proposed by Sanders et al. (1988b, 1988c). These studies have transformed our view of both the environments in which QSOs are triggered and fed and the connection between star formation and active galactic nucleus (AGN) activity.

Approximately 70% of the optically selected Palomar-Green (PG) QSO sample have *Infrared Astronomical Satellite* (*IRAS*) detections consistent with thermal emission from dust (Sanders et al. 1989). In addition, approximately a dozen low-redshift QSOs have been detected in CO(1 \rightarrow 0) to date (Sanders et al. 1988a; Barvainis et al. 1989; Alloin et al. 1992; Evans et al. 2001; Scoville et al. 2003), indicating substantial quantities of molecular gas out of which to fuel star formation and possibly AGN activity.

The detection of CO(1 \rightarrow 0) emission does not, in itself, imply that active star formation is occurring. Furthermore, in galaxies

known to harbor AGNs, it is unclear what fraction of the infrared emission is reprocessed starlight or AGN light; thus, using L_{IR} to estimate star formation rates may not be justified. The present paper addresses these issues by reporting the results of an HCN(1 \rightarrow 0) survey of QSOs previously detected in CO. HCN has a higher dipole moment and larger Einstein A -coefficient than CO, and thus traces much denser gas ($\geq 10^4 \text{ cm}^{-3}$). In the Galaxy HCN emission is associated with molecular-cloud cores where active star formation is occurring, and it has been detected in a large number of infrared luminous galaxies (Gao & Solomon 2004a). Gao & Solomon (2004b) have shown that, for spiral and infrared luminous galaxies spanning several orders in L_{IR} , the infrared-to-HCN luminosity ratio, $L_{\text{IR}}/L'_{\text{HCN}}$, is relatively constant and has smaller deviations than $L_{\text{IR}}/L'_{\text{CO}}$ measured over the same L_{IR} range. Gao & Solomon concluded that HCN is a much better tracer of the gas that ultimately gives rise to the young stellar population in these galaxies, and that the constancy of $L_{\text{IR}}/L'_{\text{HCN}}$ is also proof that the L_{IR} is due entirely to dust heating by young, massive stars. With this as a working assumption, the data presented here are used to make a comparison between the $L_{\text{IR}}/L'_{\text{HCN}}$ of the QSO host sample and the *IRAS* galaxy sample. Similarities between the $L_{\text{IR}}/L'_{\text{HCN}}$ ratios of the bulk of the *IRAS* galaxy population and those of QSO and *IRAS* galaxies with warm, AGN-like infrared colors are expected if the L_{IR} of QSO hosts and warm galaxies is due to dust heating by young, massive stars.

This paper is divided into six sections. Section 2 is a summary of the sample selection. The observing procedure and data reduction

¹ Department of Physics and Astronomy, State University of New York at Stony Brook, Stony Brook, NY 11794-3800; aevans@mail.astro.sunysb.edu, psolomon@sbastk.ess.sunysb.edu, tvavilk@vulcan.ess.sunysb.edu.

² Max-Planck-Institut für Extraterrestrische Physik, Giessenbachstrasse, Garching D-85748, Germany; linda@mpe.mpg.de.

³ Institut de Radio Astronomie Millimétrique, Domaine Universitaire, F-38406 St. Martin d’Hères, France; downes@iram.fr.

TABLE 1
SOURCE LIST

Source	R.A. (J2000.0)	Decl. (J2000.0)	D_L^a (Mpc)	z_{CO}	L_{IR}^a ($\times 10^{11} L_{\odot}$)	L_{FIR}^a ($\times 10^{11} L_{\odot}$)	SFR ^b ($M_{\odot} \text{ yr}^{-1}$)
PG 0050+124 = 1 Zw 1.....	00 53 34.94	+12 41 36.20	250	0.061	7.2	2.8	95
PG 0157+001 = Mrk 1014.....	01 59 50.21	+00 23 40.62	680	0.163	32	21	420
PG 0838+770.....	08 44 45.36	+76 53 09.20	540	0.131	2.9	1.4	40
PG 1119+120 = Mrk 734.....	11 21 47.15	+11 44 19.00	200	0.050	1.1	0.44	15
PG 1351+640.....	13 53 15.83	+63 45 45.60	360	0.088	5.6	2.1	75
PG 1415+451.....	14 17 00.84	+44 56 06.50	470	0.114	1.6	0.66	20
PG 1440+356 = Mrk 478.....	14 42 07.48	+35 26 23.10	320	0.078	2.8	1.4	40
PG 1613+658 = Mrk 876.....	16 13 57.21	+65 43 10.60	530	0.129	7.6	3.9	100
PG 2130+099 = UGC 11763.....	21 32 27.77	+10 08 19.50	250	0.063	2.1	0.62	30
Average.....							90 ± 125
Median.....							40

NOTE.—Units of right ascension are hours, minutes, and seconds, and units of declination are degrees, arcminutes, and arcseconds.

^a Calculated using the method in Sanders & Mirabel (1996) and assuming $H_0 = 75 \text{ km s}^{-1} \text{ Mpc}^{-1}$ and $q_0 = 0.5$. The L_{IR} of PG 1119+120 and PG 2130+099 are calculated using the flux densities published by Haas et al. (2003). For the remaining QSO host galaxies, the flux densities published by Sanders et al. (1989) are used.

^b Calculated by assuming that $L_{IR} = L_{SB}$ (see § 5).

are presented in § 3, followed by the results in § 4. In § 5 the infrared, CO, and HCN data of the PG QSO hosts are compared with those of both cool and warm *IRAS* galaxies to assess the relative contribution of star formation to the infrared emission of luminous AGN hosts. Section 6 is a summary of the paper. Parts of this discussion have been presented elsewhere (Evans 2003, 2006a, 2006b). Throughout this paper we adopt an $H_0 = 75 \text{ km s}^{-1} \text{ Mpc}^{-1}$ and $q_0 = 0.5$ cosmology for consistency with Evans et al. (2001, 2005).

2. SAMPLE

The sample was selected from PG QSO hosts (Schmidt & Green 1983) detected in CO(1→0) to date (see Table 1). The sample is a subset of the QSO hosts imaged at optical and near-infrared wavelengths by Surace et al. (2001) and defined to have infrared excesses (infrared-to-“big blue bump” luminosity ratio $L_{IR}[8-1000 \mu\text{m}]/L_{bb}[0.1-1.0 \mu\text{m}] > 0.36$) at least as high as those of ULIGs with warm, AGN-like infrared colors (i.e., $f_{25 \mu\text{m}}/f_{60 \mu\text{m}} \geq 0.2$; see Sanders et al. [1988c] for a discussion of the warm ULIG sample). Within the framework of the ULIG-QSO evolutionary model, infrared-excess PG QSO hosts represent the stage following the warm, AGN-like ULIG phase, and thus their hosts should still show signatures consistent with ultraluminous, gas-rich galaxy mergers (tidal tails, young star clusters, molecular gas, etc.). Given this, they are also the most likely QSO hosts to have the highest contribution of starlight to the production of their infrared luminosity. The reader is referred to Surace et al. (2001) for a more detailed discussion of the sample selection.

For the purposes of the study presented here, the QSOs listed in Table 1 have three primary advantages. First, the CO redshifts and line widths are known, thus making it straightforward to tune to the frequency of the HCN line and, in the absence of a strong HCN line, to measure upper limits. Second, *IRAS* and *Infrared Space Observatory* data have been published for these QSOs, making determinations of the infrared luminosity possible (Table 1). Third, because of the manner in which they are selected, they are directly comparable to the warm *IRAS* galaxy sample.

3. OBSERVATIONS AND DATA REDUCTION

Observations of the redshifted HCN emission were done at the IRAM 30 m telescope during five observing periods between 2003 May and 2003 December (see Table 2). The 3 and 2 mm

receivers were used in combination with the filter-banks and an autocorrelator to provide bandwidths of 512 and 600 MHz, respectively. All QSO hosts with HCN(1 → 0) emission redshifted to frequencies accessible with the 3 mm receivers were observed in HCN(1 → 0); otherwise, HCN(2 → 1) observations were obtained with the 2 mm receiver. During observations the pointing was monitored by observing standard continuum sources.

Three additional sets of observations were obtained. First, all of the QSOs were observed in CO(1 → 0) during the 2003 December and 2006 May observing periods to verify CO redshifts and line widths. Second, observations of the HCN(1 → 0) emission from Arp 220 and the CO(1 → 0) emission from VII Zw 031 were made after every other QSO observation as a reality check of the 30 m telescope system performance. Finally, Arp 220 was observed in HCN(1 → 0) and HCN(2 → 1) to measure the ratio of two lines (see § 4).

The data were reduced using the IRAM data reduction package CLASS. Scans were averaged together, and a linear baseline was subtracted from each spectrum outside of the velocity range

TABLE 2
JOURNAL OF OBSERVATIONS

Source	Transition	Date	Time (hr)	T_{sys} (K)
PG 0050+124.....	CO(1 → 0)	2003 Dec	40	161
	HCN(1 → 0)	2003 May	527	102
	HCN(1 → 0)	2003 Sep	215	111
PG 0157+001.....	CO(1 → 0)	2003 Dec	50	111
	HCN(1 → 0)	2003 Dec	70	260
PG 0838+770.....	CO(1 → 0)	2003 Dec	45	111
	HCN(2 → 1)	2003 May	220	217
PG 1119+120.....	CO(1 → 0)	2003 Dec	67	95
	HCN(1 → 0)	2003 Jun	301	108
PG 1351+640.....	CO(1 → 0)	2006 May	98	146
	HCN(1 → 0)	2003 Jun	300	111
PG 1415+451.....	CO(1 → 0)	2003 Dec	50	106
	HCN(1 → 0)	2003 Dec	205	116
PG 1440+356.....	CO(1 → 0)	2003 Dec	80	126
	HCN(1 → 0)	2003 Dec	210	120
PG 1613+658.....	CO(1 → 0)	2003 Dec	35	126
	HCN(2 → 1)	2003 Dec	125	235
PG 2130+099.....	CO(1 → 0)	2003 Dec	140	157

of the CO and HCN line emission, or, in the cases for which no HCN line was detected, outside the velocity range where the HCN line was expected to be. The amplitudes of each spectrum were converted to main-beam brightness temperatures, T_{mb} , by multiplying the spectrum by the ratio of the forward-to-beam efficiencies of the telescope at the specific frequency of the observation and then smoothing each spectrum to $\sim 20 \text{ km s}^{-1}$. Finally, line fluxes were measured by numerically integrating over the channels in the line profile, and the line widths were measured as full width at 50% of the peak flux. The resulting spectra are plotted in Figures 1–3.

4. RESULTS

4.1. CO

Table 3 contains a summary of the CO emission-line properties of the sample of PG QSO hosts. The CO luminosities are calculated via

$$L'_{\text{CO}} = 2.4 \times 10^3 \left(\frac{S_{\text{CO}} \Delta v}{1 \text{ Jy km s}^{-1}} \right) \left(\frac{D_L}{1 \text{ Mpc}} \right)^2 \times (1+z)^{-1} \text{ K km s}^{-1} \text{ pc}^2, \quad (1)$$

where $S_{\text{CO}} \Delta v$ is the CO flux obtained by multiplying the line intensities in Table 3 by the conversion factor for an unresolved source (i.e., $S/T_{\text{mb}} = 4.95 \text{ J K}^{-1}$) and D_L is the luminosity distance. The molecular gas masses, M_{H_2} , are calculated by adopting the conversion factor $\alpha = M(\text{H}_2)/L'_{\text{CO}} = 4 M_{\odot} (\text{K km s}^{-1} \text{ pc}^2)^{-1}$ (see Evans et al. 2001 for a detailed discussion of α).

There is considerable overlap between the QSOs listed in Table 3 and recent interferometric surveys with the Owens Valley Millimeter Array at the Owens Valley Radio Observatory (OVRO). Specifically, PG 0838+770, PG 1119+120, PG 1351+640, PG 1415+451, PG 1440+356, and PG 1613+658 were observed by Evans et al. (2001), and PG 2130+099 was observed as part of a volume-limited ($z < 0.1$) QSO CO survey by Scoville et al. (2003). In addition, previous single-dish measurements of CO emission from I Zw 1, Mrk 1014, PG 0838+770, and PG 1613+658 exist (Sanders et al. 1988a; Barvainis et al. 1989; Alloin et al. 1992).

The general shape and width of the CO lines are consistent with previously published CO spectra of these QSOs. For the QSOs with broad ($> 200 \text{ km s}^{-1}$) CO emission lines, the CO velocity width measured at half the maximum intensity, Δv_{FWHM} , agrees to within 20% of prior measurements. The agreement degrades to 40% for the narrow ($< 100 \text{ km s}^{-1}$) CO line QSOs, the larger discrepancy resulting from the difficulty in accurately measuring Δv_{FWHM} for narrow emission lines after rebinning the data. From these new measurements, an average CO emission line of $\Delta v_{\text{FWHM}} \sim 280 \pm 150 \text{ km s}^{-1}$ is estimated, as compared to the value of $300 \pm 90 \text{ km s}^{-1}$ measured for ULIGs (see Solomon et al. 1997; Evans et al. 2005).

With the exception of PG 1613+658, the new measurements of main-beam CO line fluxes, $S_{\text{CO}} \Delta v$, are on average 40% lower than the OVRO data presented in Evans et al. (2001). The new CO line flux measurement of PG 1613+658, which is the PG QSO with the highest signal-to-noise ratio CO detection in Evans et al. (2001), agrees to within 4% with the OVRO data. Finally, the CO line flux of PG 2130+099 agrees to within 10% of the measurement made by Scoville et al. (2003).

While previous single-dish $S_{\text{CO}} \Delta v$ measurements of I Zw 1 and PG 1613+658 are consistent to within 20% of the measurements presented here, single-dish measurements of PG 0838+770 and Mrk 1014 are up to 300% higher than the present

measurements. The discrepancies are undoubtedly a result of calibration errors and low signal-to-noise ratio data.

4.2. HCN

Table 3 also summarizes the HCN emission-line properties of the QSO sample and Arp 220. Only the PG QSO host I Zw 1 was detected in HCN($1 \rightarrow 0$); the shape and width of the HCN line are consistent with the CO($1 \rightarrow 0$) profile. For the remaining PG QSO hosts, the HCN line intensities were measured by numerically integrating over the channels expected to contain HCN emission based on the CO($1 \rightarrow 0$) observations. In addition, 3σ upper limits to the HCN line intensities were derived via

$$T_{\text{HCN}} \Delta v < \frac{3T_{\text{rms}} \Delta v_{\text{FWZI}}}{\sqrt{\Delta v_{\text{FWZI}} / \Delta v_{\text{res}}}} \text{ K km s}^{-1}, \quad (2)$$

where Δv_{FWZI} is the full width at zero intensity velocity of the CO emission line of the QSO host and T_{rms} is the rms main-beam temperature of the HCN spectral data for a velocity resolution of Δv_{res} . Line luminosities were calculated via

$$L'_{\text{HCN}(J \rightarrow J-1)} = 4.145 \times 10^3 \left(\frac{S_{\text{HCN}} \Delta v}{1 \text{ Jy km s}^{-1}} \right) \left(\frac{D_L}{1 \text{ Mpc}} \right)^2 \times J^{-2} (1+z)^{-1} \text{ K km s}^{-1} \text{ pc}^2. \quad (3)$$

The HCN($1 \rightarrow 0$) lines of two of the PG QSOs (PG 0838+770 and PG 1613+658) are redshifted to frequencies below the range accessible with the 3 mm receivers. In both cases, the 2 mm receivers were tuned to the frequencies corresponding to the redshifted HCN($2 \rightarrow 1$) emission line. Both observations resulted in upper limits, which were converted to HCN($1 \rightarrow 0$) upper limits by adopting the $L'_{\text{HCN}(1 \rightarrow 0)}/L'_{\text{HCN}(2 \rightarrow 1)}$ ($= 2.997$) line ratio measured for Arp 220 (Fig. 3).

5. DISCUSSION

Approximately one-quarter of the PG QSOs at $z < 0.3$ have been detected in CO($1 \rightarrow 0$), and $\sim 50\%$ – 70% show evidence of spiral disks, merger-like tidal features, and/or luminous star clusters (e.g., Stockton & MacKenty 1983; Surace et al. 2001 and references therein; Veilleux et al. 2006; Guyon et al. 2006). The presence of star-forming molecular gas and luminous star clusters, combined with infrared luminosities in excess of $10^{11} L_{\odot}$, are compelling indications that star formation is an important component of activity in these galaxies, and it raises the possibility that a significant fraction of their thermal infrared emission may be reprocessed stellar light.

Given such evidence, an obvious question to ask is: What are the star formation rates of the PG QSO hosts? As a naive first attempt, the assumption is made that the infrared luminosity of the host is due entirely to dust heating by the starburst population, and that $\tau \gg 1$ toward the star-forming regions. Doing so yields star formation rates of

$$\text{SFR} \sim 1.32 \times 10^{-10} \left(\frac{L_{\text{IR}}}{1 L_{\odot}} \right) \left(\frac{\delta}{0.75} \right) M_{\odot} \text{ yr}^{-1} \sim 20\text{--}420 M_{\odot} \text{ yr}^{-1}, \quad (4)$$

with an average star formation rate of $\langle \text{SFR} \rangle \sim 90 \pm 125 M_{\odot} \text{ yr}^{-1}$ and the median of $40 M_{\odot} \text{ yr}^{-1}$ (Table 1). Equation (4) is a modified version of equation (4) in Kennicutt (1998), where the factor δ ($= 0.75 \pm 0.07$) is the average far-infrared-to-infrared luminosity ratio, $L_{\text{FIR}}(40\text{--}500 \mu\text{m})/L_{\text{IR}}(8\text{--}1000 \mu\text{m})$, calculated for

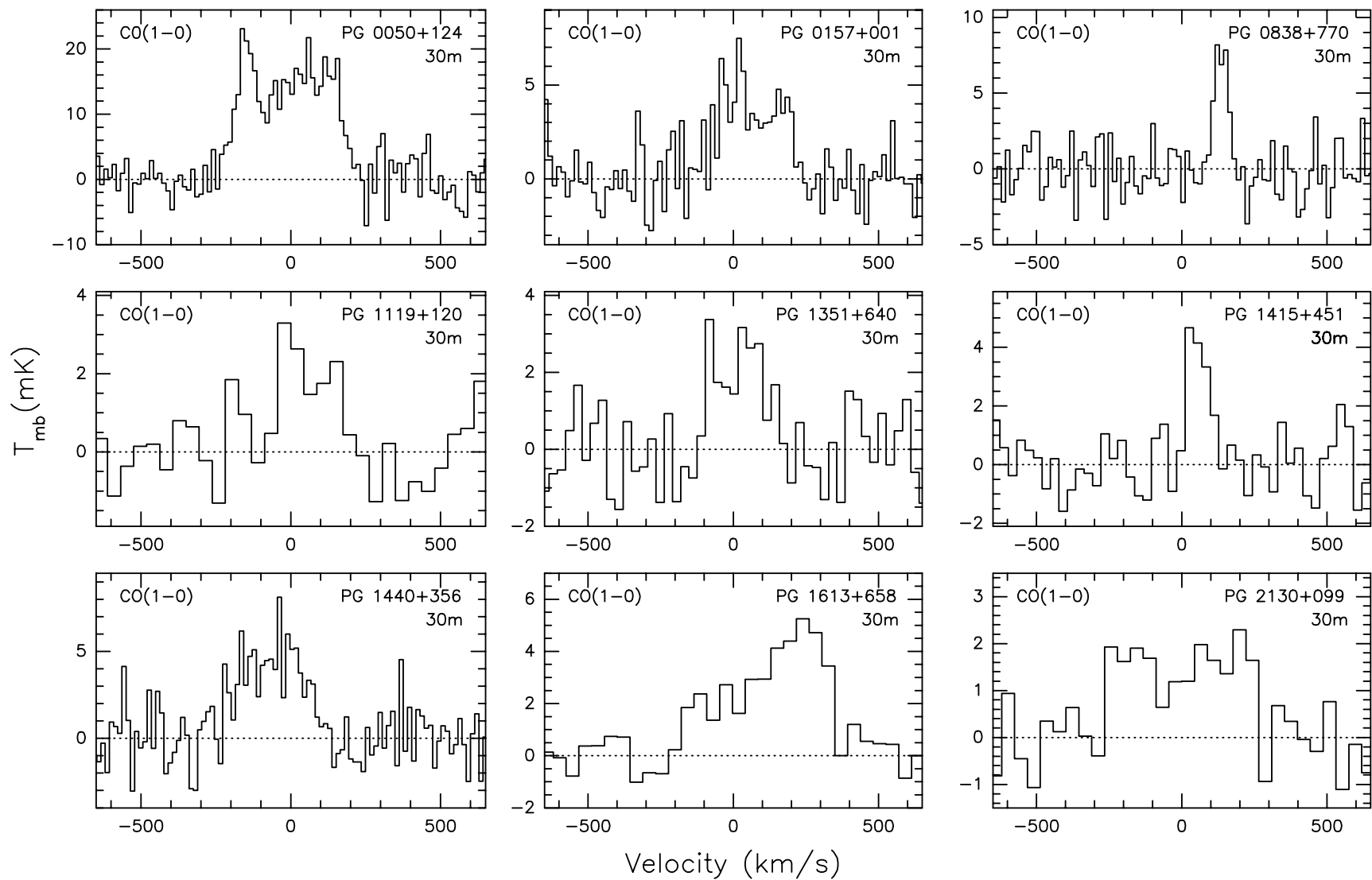


FIG. 1.—IRAM 30 m spectra of CO(1 \rightarrow 0) emission from nine PG QSO hosts with infrared excesses. The intensity scale is in units of main-beam brightness temperature. A linear baseline has been subtracted from each spectrum; the baseline subtraction is performed outside of the velocity range of the emission lines. The zero velocity corresponds to the redshifts listed in Table 1.

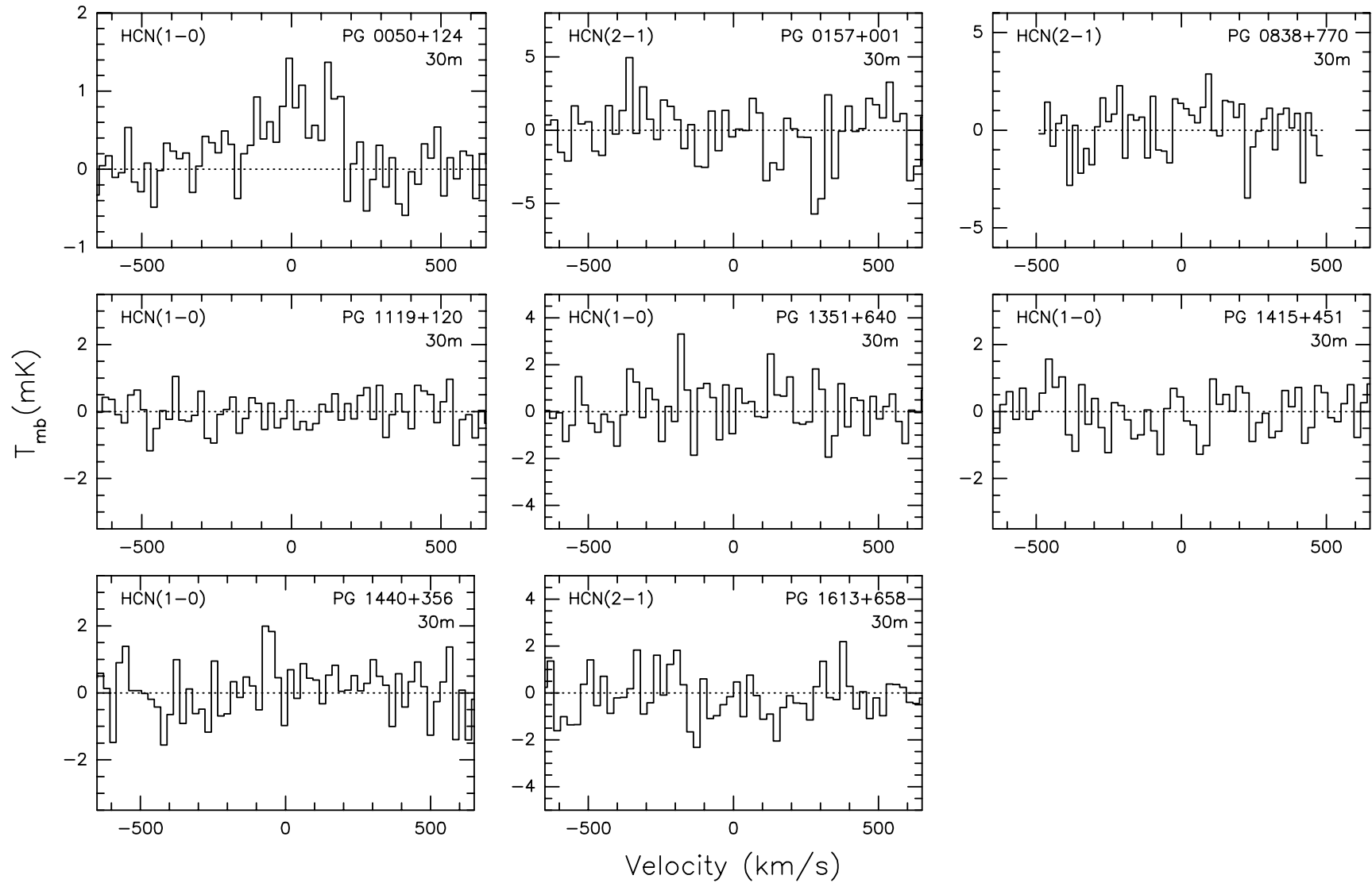


FIG. 2.—IRAM 30 m spectra of HCN($1 \rightarrow 0$) and HCN($2 \rightarrow 1$) emission from the QSO host sample. The intensity scale is in units of main-beam brightness temperature. A linear baseline has been subtracted from each spectrum; the baseline subtraction is performed outside of the velocity range where the emission line is expected to be based on the position and velocity width of CO($1 \rightarrow 0$) emission from these QSO hosts.

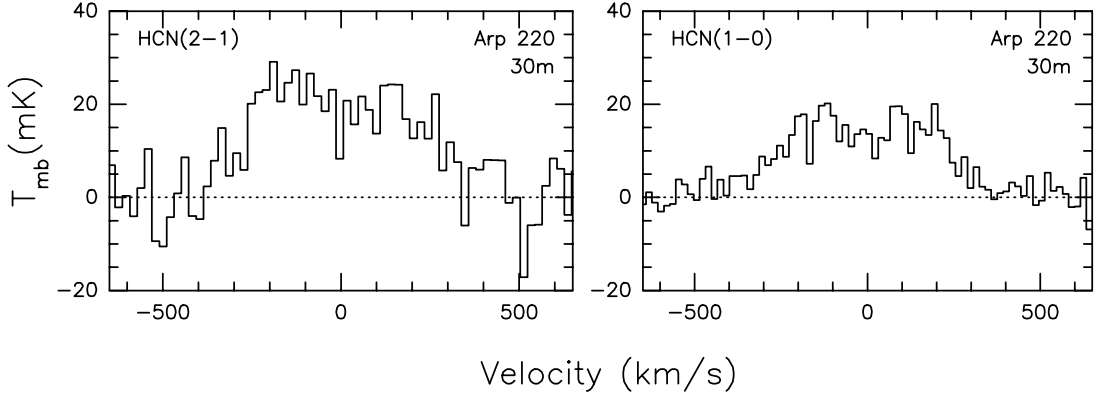


FIG. 3.—IRAM 30 m spectra of HCN(1 \rightarrow 0) and HCN(2 \rightarrow 1) emission from the ULIG Arp 220. The intensity scale is in units of main-beam brightness temperature. A linear baseline has been subtracted from each spectrum; the baseline subtraction is performed outside of the velocity range of the emission lines. The zero velocity corresponds to a redshift of 0.0181.

the *IRAS* galaxies in the Revised Bright Galaxy Sample (~ 600 galaxies; Sanders et al. 2003). These star formation rates are likely upper limits; it is difficult to imagine a geometry in which light from the AGN does not intersect (and thus heat) a significant fraction of dust in the host galaxy. Indeed, models have been developed that can account for all of the infrared emission in QSO hosts by an AGN surrounded by a warped or clumpy torus (Sanders et al. 1989; see review in Haas et al. 2003; Elitzur et al. 2004).

5.1. $L_{\text{IR}}/L'_{\text{CO}}$: Star Formation Efficiencies versus Dust Heating by the AGN

To examine the importance of dust heating by young, massive stars to the production of L_{IR} in their hosts, consider first the L'_{CO} and L_{IR} of QSO hosts relative to that of *IRAS*-detected galaxies

(Fig. 4; see also Evans et al. 2001, 2005). The new L'_{CO} measurements of the infrared-excess QSO hosts (Table 3) are plotted in Figure 4;⁴ additional QSO data are compiled from Scoville et al. (2003). In order to provide a more meaningful comparison with the QSO hosts the *IRAS* galaxies have been separated into those with warm, Seyfert-like (i.e., $f_{25\ \mu\text{m}}/f_{60\ \mu\text{m}} \geq 0.20$) and cool ($f_{25\ \mu\text{m}}/f_{60\ \mu\text{m}} < 0.20$) infrared colors. There is significant evidence that most warm *IRAS* galaxies host AGNs, but there is not clear evidence that cool *IRAS* galaxies, as a class, have luminous

⁴ Note that Evans et al. (2001) used $L_{\text{IR}}(1-1000\ \mu\text{m})$ for QSO hosts instead of the commonly used $L_{\text{IR}}(8-1000\ \mu\text{m})$. The $L_{\text{IR}}(1-1000\ \mu\text{m})$ values in Evans et al. (2001) were calculated by numerically integrating the spectral energy distributions in Sanders et al. (1989). Here, we use $L_{\text{IR}}(8-1000\ \mu\text{m})$, which leaves out the significant contribution of hot dust in the 1–8 μm range but provides better consistency with the other data sets plotted.

TABLE 3
EMISSION-LINE PROPERTIES

Source	z_{CO}	Line	Δv_{FWHM} (km s^{-1})	$T_{\text{mb}}\Delta v$ (K km s^{-1})	$S_{\text{line}}\Delta v$ (Jy km s^{-1})	L'_{line} ^{a,b} ($\text{K km s}^{-2} \text{pc}^2$)	$M(\text{H}_2)$ ^c (M_{\odot})	$L_{\text{IR}}/L'_{\text{line}}$ ^d	$L_{\text{IR}}/L'_{\text{HCN}(1-0)}$ ^{d,e}
PG 0050+124.....	0.061	CO(1 \rightarrow 0)	370	6.0 ± 0.2	30 ± 1.1	4.2×10^9	1.7×10^{10}	170	...
	0.061	HCN(1 \rightarrow 0)	290	0.27 ± 0.03	1.3 ± 0.1	3.2×10^8	...	2260	...
PG 0157+001.....	0.163	CO(1 \rightarrow 0)	270	1.1 ± 0.1	5.5 ± 0.5	5.2×10^9	2.1×10^{10}	610	...
	...	HCN(1 \rightarrow 0)	...	-0.12 ± 0.16	-0.60 ± 0.80	$<9.6 \times 10^8$...	>3300	>1100
PG 0838+770.....	0.132	CO(1 \rightarrow 0)	60	0.50 ± 0.07	2.5 ± 0.4	1.5×10^9	6.1×10^9	190	...
	...	HCN(2 \rightarrow 1)	...	0.12 ± 0.06	0.60 ± 0.31	$<1.8 \times 10^8$...	>1590	>530
PG 1119+120.....	0.050	CO(1 \rightarrow 0)	220	0.54 ± 0.09	2.7 ± 0.4	2.5×10^8	1.0×10^9	450	...
	...	HCN(1 \rightarrow 0)	...	-0.01 ± 0.04	-0.05 ± 0.19	$<9.2 \times 10^7$...	>1230	...
PG 1351+640.....	0.088	CO(1 \rightarrow 0)	260	0.54 ± 0.09	2.7 ± 0.5	7.7×10^8	3.1×10^9	730	...
	...	HCN(1 \rightarrow 0)	...	0.09 ± 0.08	0.46 ± 0.40	$<5.5 \times 10^8$...	>1000	...
PG 1415+451.....	0.114	CO(1 \rightarrow 0)	90	0.42 ± 0.06	2.1 ± 0.3	9.8×10^8	3.9×10^9	160	...
	...	HCN(1 \rightarrow 0)	...	-0.02 ± 0.04	-0.12 ± 0.20	$<3.8 \times 10^8$...	>420	...
PG 1440+356.....	0.078	CO(1 \rightarrow 0)	310	1.3 ± 0.1	6.6 ± 0.6	1.5×10^9	6.0×10^9	190	...
	...	HCN(1 \rightarrow 0)	...	0.09 ± 0.08	0.43 ± 0.40	$<3.9 \times 10^8$...	>720	...
PG 1613+658.....	0.129	CO(1 \rightarrow 0)	400	1.6 ± 0.1	8.0 ± 0.6	4.8×10^9	1.9×10^{10}	160	...
	...	HCN(2 \rightarrow 1)	...	-0.17 ± 0.13	-0.83 ± 0.63	$<4.1 \times 10^8$...	>1850	>620
PG 2130+099.....	0.063	CO(1 \rightarrow 0)	530	0.78 ± 0.1	3.9 ± 0.5	5.6×10^8	2.2×10^9	380	...
Arp 220.....	0.0181	HCN(1 \rightarrow 0)	550	9.0 ± 0.8	45 ± 3	9.6×10^8	...	1450	...
	...	HCN(2 \rightarrow 1)	550	12 ± 1.4	60 ± 7	3.2×10^8
PG QSO average (CO).....			260 \pm 150						

^a 3 σ upper limit.

^b Calculated assuming $H_0 = 75 \text{ km s}^{-1} \text{ Mpc}^{-1}$ and $q_0 = 0.5$.

^c Calculated assuming $\alpha = 4 M_{\odot} (\text{K km s}^{-1} \text{pc}^2)^{-1}$.

^d In units of $L_{\odot} (\text{K km s}^{-1} \text{pc}^2)^{-1}$.

^e $L'_{\text{HCN}(2-1)}/L'_{\text{HCN}(1-0)}$ conversion is achieved by adopting the $L'_{\text{HCN}(1-0)}/L'_{\text{HCN}(2-1)}$ (≈ 2.997) of Arp 220. See § 4.2.

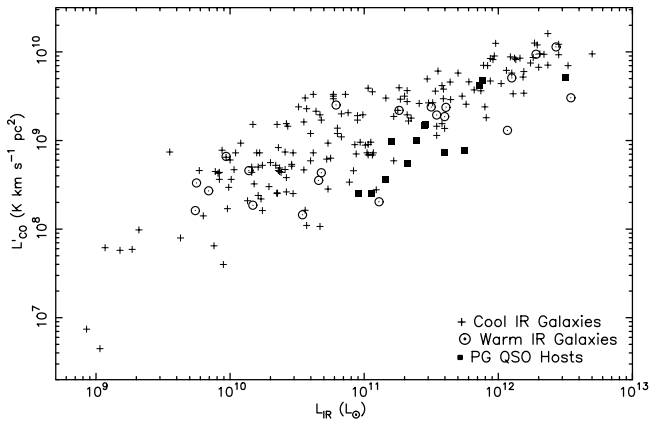


FIG. 4.— L'_{CO} vs. L_{IR} of the PG QSO hosts and a sample of *IRAS*-detected galaxies. Infrared galaxy data come from Mazzarella et al. (1993) and Solomon et al. (1997), and PG QSO host data come from this paper and Scoville et al. (2003).

AGNs. Given this, the cool galaxies are treated as galaxies powered by starbursts.

The new CO data show results similar to what is shown in Evans et al. (2001, 2005); the QSO hosts have low L'_{CO} for their L_{IR} relative to the bulk of cool *IRAS* galaxies. In other words, QSO hosts have high $L_{\text{IR}}/L'_{\text{CO}}$ relative to cool *IRAS* galaxies with comparable L_{IR} . The warm galaxies with $L_{\text{IR}} > 10^{10.0} L_{\odot}$ show a similar trend in $L_{\text{IR}}/L'_{\text{CO}}$ relative to the cool *IRAS* sample, although not as dramatically as the QSO host population.

To interpret the data plotted in Figure 4, consider

$$\frac{L_{\text{IR}}}{L'_{\text{CO}}} \sim \frac{L_{\text{SB}} + \epsilon L_{\text{AGN}}}{(M_{\text{H}_2}/\alpha)}, \quad (5)$$

where L_{SB} and L_{AGN} are the luminosities of the starburst and AGN, respectively, and ϵ is the fraction of the AGN light absorbed by dust and reradiated in the thermal infrared. In the limit where either $L_{\text{AGN}} = 0$ or $\epsilon = 0$, equation (5) is simply the star formation efficiency; i.e., if $\tau \gg 1$ toward the starburst population that is producing stars in steady state, $L_{\text{IR}}/L'_{\text{CO}}$ is a measure of total energy output of the starburst population per unit of fuel available to form new stars. If $\epsilon = 0$ for QSO hosts, then the high $L_{\text{IR}}/L'_{\text{CO}}$ is an indication that they are producing stars extremely efficiently from the available molecular gas. Indeed, one would be forced to conclude that the star formation efficiency is preferentially higher in galaxies hosting luminous AGNs. The alternative interpretation is that $\epsilon > 0$, and thus that ϵL_{AGN} contributes significantly to L_{IR} .

5.2. Dense Molecular Gas and Star Formation Rates

The conclusions stated in the above discussion are only valid if CO is a robust tracer of star formation in these galaxies, i.e., if the CO emission is tracing most, if not all, of the molecular hydrogen that is actively forming stars. Given that HCN appears to be more closely coupled with star formation in starburst galaxies than CO (see § 1), applying a similar analysis to HCN as done in § 5.1 for CO will likely yield a more physically meaningful result.

Figure 5 is a plot of $L_{\text{IR}}/L'_{\text{HCN}}$ versus L_{IR} of the QSO hosts, *IRAS* galaxies, and two high-redshift AGNs recently detected in HCN ($1 \rightarrow 0$). Again, the *IRAS* galaxies have been separated into those with warm and cool infrared colors. If the dust in the cool *IRAS* galaxies is heated primarily by the starburst population

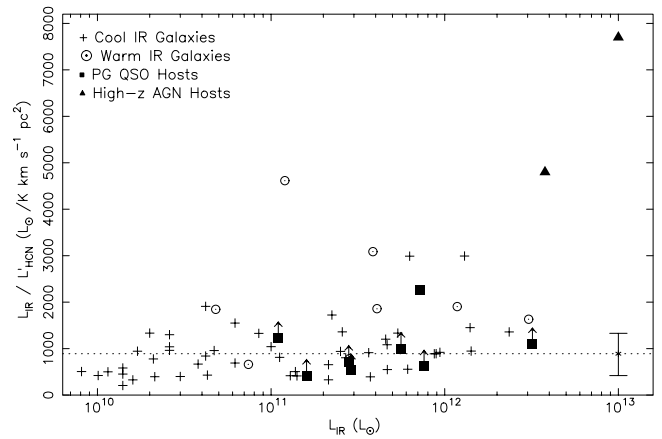


FIG. 5.— $L_{\text{IR}}/L'_{\text{HCN}}$ vs. L_{IR} of the PG QSO hosts, a sample of local *IRAS* galaxies, and two high- z AGNs (FSC 10214+4724 and the Cloverleaf Quasar). Squares with arrows represent 3σ $L_{\text{IR}}/L'_{\text{HCN}}$ lower limits of the PG QSOs not detected in HCN. The dashed line is $L_{\text{IR}}/L'_{\text{HCN}} = 890 L_{\odot} (\text{K km s}^{-1} \text{pc}^2)^{-1}$ (see § 5.1); the error bar associated with the dashed line encloses 67% (1σ) of the cool galaxy data points. With the exception of NGC 4418 (Imanishi et al. 2004), Mrk 273 and IR 17208–0014 (Imanishi et al. 2006), and Arp 220 (this paper), the *IRAS* galaxy HCN data are compiled from Gao & Solomon (2004a, 2004b). The F10214+4724 and Cloverleaf data are from Vanden Bout et al. (2004) and Solomon et al. (2003), respectively.

($\epsilon \sim 0$), then the median $L_{\text{IR}}/L'_{\text{HCN}}$ of the cool *IRAS* sample is adopted as the ratio at which $L_{\text{IR}} = L_{\text{SB}}$; i.e.,

$$\left\langle \frac{L_{\text{IR}}}{L'_{\text{HCN}}} \right\rangle_{\text{cool}} \sim \frac{L_{\text{SB}}}{(M_{\text{H}_2}/\alpha_{\text{HCN}})} \sim 890_{-470}^{+440} L_{\odot} (\text{K km s}^{-1} \text{pc}^2)^{-1}, \quad (6)$$

where α_{HCN} is the L'_{HCN} -to- M_{H_2} mass conversion factor and the limits on $\langle L_{\text{IR}}/L'_{\text{HCN}} \rangle_{\text{cool}}$ represent the range in which 67% (i.e., 1σ) of the data points around the median are contained.

The upper portion of Figure 5 (i.e., high $L_{\text{IR}}/L'_{\text{HCN}}$) is mostly populated with the warm galaxies and AGN hosts. Specifically, the QSO host I Zw 1, the two high-redshift AGN hosts, and two of the eight warm *IRAS* galaxies have much higher $L_{\text{IR}}/L'_{\text{HCN}}$ (>2200) than the cool galaxy population (i.e., low values of L'_{HCN} for their L_{IR}). These galaxies clearly have a significant contribution to their L_{IR} from AGN activity. Further, the fact that both of the cool *IRAS* galaxies within this $L_{\text{IR}}/L'_{\text{HCN}}$ range (Arp 299 and Mrk 273, for which $L_{\text{IR}}/L'_{\text{HCN}} \sim 3000$) have strong X-ray signatures of embedded AGNs (Della Ceca et al. 2002; Xia et al. 2002; Zesas et al. 2003) also supports the idea that high $L_{\text{IR}}/L'_{\text{HCN}}$ ratios are the result of significant dust heating by AGNs. Four of the eight warm galaxies have $L_{\text{IR}}/L'_{\text{HCN}}$ in the range 1600–2000, and thus overlap the high end of the bulk of the cool galaxy distribution. These galaxies, which include the well-studied ULIG Mrk 231, might have an equal mixture of AGN and starburst emission as viewed in the thermal infrared; however, they could also be almost entirely powered by star formation, as their $L_{\text{IR}}/L'_{\text{HCN}}$ is not outside the range of that found in cool galaxies. Finally, two of the eight warm galaxies have $L_{\text{IR}}/L'_{\text{HCN}}$ very near the median of the cool galaxy population, illustrating the fact that some fraction of the warm galaxy population have “normal” $L_{\text{IR}}/L'_{\text{HCN}}$. Whether or not the PG QSO hosts not detected in HCN have high $L_{\text{IR}}/L'_{\text{HCN}}$ similar to I Zw 1 cannot be addressed with the data in Figure 5.

While only one of the eight PG QSO hosts was detected in HCN, and the $L_{\text{IR}}/L'_{\text{HCN}}$ lower limits of the undetected QSO hosts are not sufficiently constraining to be conclusive, the $L_{\text{IR}}/L'_{\text{HCN}}$ ratios

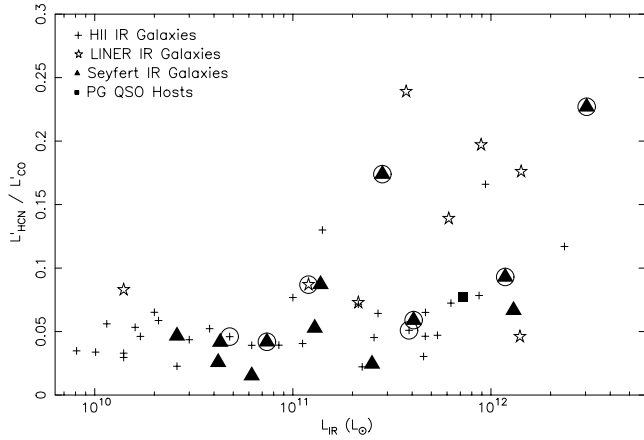


FIG. 6.— $L'_{\text{HCN}}/L'_{\text{CO}}$ vs. L_{IR} for 1 Zw 1 and *IRAS* galaxies. The *IRAS* galaxy data are plotted by their optical emission-line classification. The warm *IRAS* galaxies are circled.

of the undetected hosts can possibly be inferred by making use of the larger number of HCN-detected Seyfert galaxies in the *IRAS* galaxy sample. Figure 6 is a plot of $L'_{\text{HCN}}/L'_{\text{CO}}$ versus L_{IR} , and is a modified version of Figure 4 in Gao & Solomon (2004b). Here, the *IRAS* galaxies have been plotted in terms of their optical emission-line classifications (i.e., Seyfert, LINER [low-ionization nuclear emission region], and H II region-like galaxies). In this figure there is an increased spread in $L'_{\text{HCN}}/L'_{\text{CO}}$ values for galaxies with $L_{\text{IR}} > 10^{11} L_{\odot}$, which Gao & Solomon (2004b) attribute to the increase in the fraction of dense gas in luminous infrared galaxies corresponding to the increase in starburst activity. Eleven of the 13 (85%) Seyfert galaxies in Figure 6 have $L'_{\text{HCN}}/L'_{\text{CO}} < 0.1$. In addition, 1 Zw 1 has an $L'_{\text{HCN}}/L'_{\text{CO}}$ ratio within the distribution of Seyfert galaxy data points at $L'_{\text{HCN}}/L'_{\text{CO}} < 0.1$.

Given this, it is a reasonable assumption that the PG QSO hosts in the present sample have low $L'_{\text{HCN}}/L'_{\text{CO}}$ similar to the bulk of the Seyfert galaxies in Figure 6. Thus, for the PG QSO hosts, the median $L'_{\text{HCN}}/L'_{\text{CO}}$ of Seyfert galaxies and 1 Zw 1 in Figure 6, i.e.,

$$\left\langle \frac{L'_{\text{HCN}}}{L'_{\text{CO}}} \right\rangle_{\text{Seyfert}} \sim 0.06^{+0.03}_{-0.04}, \quad (7)$$

is adopted, where the uncertainties span the range of $L'_{\text{HCN}}/L'_{\text{CO}}$ for the 11 low $L_{\text{HCN}}/L'_{\text{CO}}$ Seyfert galaxies. A direct estimation of $L_{\text{IR}}/L'_{\text{HCN}}$ for the QSO hosts can then be made from the $L_{\text{IR}}/L'_{\text{CO}}$ of the QSO hosts listed in Table 3. The resulting $L_{\text{IR}}/L'_{\text{HCN}}$ ratios are listed in Table 4, and the data are plotted in Figure 7. The stellar contributions to the production of L_{IR} of PG QSOs hosts is thus

$$\begin{aligned} \Delta_{\text{SB}}(\text{IR}) &\sim 5340 \left(\frac{\langle L_{\text{IR}}/L'_{\text{HCN}} \rangle_{\text{cool}}}{890} \right) \\ &\times \left(\frac{\langle L'_{\text{HCN}}/L'_{\text{CO}} \rangle_{\text{Seyfert}}}{0.06} \right) \\ &\times \left(\frac{L_{\odot} [\text{K km s}^{-1} \text{ pc}^2]^{-1}}{L_{\text{IR}}/L'_{\text{CO}}} \right) \% \\ &\sim 7\% - 39\%, \end{aligned}$$

and the star formation rates are $2-37 M_{\odot} \text{ yr}^{-1}$ (median = $10 M_{\odot} \text{ yr}^{-1}$). Note, however, that given the uncertainties in equation (7), the possibility that massive, young stars produce 60% of L_{IR} cannot be ruled out for 50% of the QSOs plotted in Figure 7. By comparison, the corresponding values for the warm galaxies are $\sim 10\% - 100\%$ and $\sim 3-220 M_{\odot} \text{ yr}^{-1}$ (median = $20 M_{\odot} \text{ yr}^{-1}$), respectively.

TABLE 4
INFRARED-TO-HCN LUMINOSITY RATIO COMPARISONS AND ADJUSTED STAR FORMATION RATES

Source	Type	Class ^a	$L_{\text{IR}}/L'_{\text{HCN}}$ ^b	$L_{\text{FIR}}/L'_{\text{HCN}}$ ^b	$\langle L_{\text{IR}}/L'_{\text{HCN}} \rangle_{\text{cool}} / (L_{\text{IR}}/L'_{\text{HCN}})$	$\langle L_{\text{FIR}}/L'_{\text{HCN}} \rangle_{\text{cool}} / (L_{\text{FIR}}/L'_{\text{HCN}})$	SFR ^c
Median	Cool	...	890^{+440}_{-470}	660^{+370}_{-330}
Median	Warm	...	1850^{+1240}_{-1070}	1220^{+860}_{-810}	0.48 ± 0.25	0.54 ± 0.28	...
Median	QSO	...	3150^{+6300}_{-1050}	1575^{+4720}_{-530}	$0.28^{+0.35}_{-0.24}$	$0.42^{+0.56}_{-0.35}$...
PG 1351+640.....	QSO	Seyfert 1	12120^{+24230}_{-4040}	4540^{+9090}_{-1520}	$0.07^{+0.09d}_{-0.06}$	$0.15^{+0.19d}_{-0.12}$	5^{+7}_{-5}
PG 0157+001.....	QSO	Seyfert 1	10120^{+20230}_{-3370}	6640^{+13280}_{-2210}	$0.09^{+0.11d}_{-0.07}$	$0.10^{+0.13d}_{-0.08}$	37^{+46}_{-31}
PG 1119+120.....	QSO	Seyfert 1	7530^{+15070}_{-2510}	3010^{+6030}_{-1000}	$0.12^{+0.15d}_{-0.10}$	$0.22^{+0.29d}_{-0.18}$	2^{+2}_{-1}
Cloverleaf Quasar	High- <i>z</i> AGN	Seyfert 1	7700	1700	0.12 ± 0.06	0.39 ± 0.20	375 ± 190
PG 2130+099	QSO	Seyfert 1	6250^{+12500}_{-2080}	1840^{+3690}_{-610}	$0.14^{+0.18d}_{-0.12}$	$0.36^{+0.48d}_{-0.30}$	4^{+5}_{-3}
IRAS FSC 10214+4724.....	High- <i>z</i> AGN	Seyfert 2	4800	2600	0.19 ± 0.10	0.25 ± 0.13	223 ± 110
NGC 4418.....	Warm	LINER	4610	3830	0.19 ± 0.10	0.17 ± 0.09	3 ± 2
PG 1440+356.....	QSO	Seyfert 1	3150^{+6300}_{-1050}	1580^{+3150}_{-520}	$0.28^{+0.35d}_{-0.24}$	$0.42^{+0.56d}_{-0.35}$	10^{+13}_{-9}
PG 0838+770.....	QSO	Seyfert 1	3150^{+6300}_{-1050}	1520^{+3040}_{-510}	$0.28^{+0.35d}_{-0.24}$	$0.43^{+0.58d}_{-0.36}$	11^{+13}_{-9}
PG 1415+451.....	QSO	Seyfert 1	2720^{+5430}_{-910}	1120^{+2240}_{-370}	$0.33^{+0.41d}_{-0.28}$	$0.59^{+0.79d}_{-0.49}$	7^{+9}_{-6}
PG 1613+658.....	QSO	Seyfert 1	2630^{+5270}_{-880}	1380^{+2760}_{-460}	$0.34^{+0.42d}_{-0.28}$	$0.48^{+0.64d}_{-0.40}$	34^{+42}_{-29}
NGC 1614.....	Warm	H II/LINER	3090	2090	0.29 ± 0.15	0.32 ± 0.17	15 ± 7
PG 0050+124 = 1 Zw 1	QSO	Seyfert 1	2260	880	0.39 ± 0.20	0.75 ± 0.39	37 ± 19
IRAS FSC 05189-2524.....	Warm	Seyfert 2	1900	1260	0.47 ± 0.24	0.52 ± 0.28	73 ± 37
NGC 7469.....	Warm	Seyfert 1	1860	1190	0.48 ± 0.25	0.55 ± 0.29	26 ± 13
NGC 3034 = M82	Warm	H II	1850	1270	0.48 ± 0.25	0.52 ± 0.27	3 ± 2
Mrk 231	Warm	Seyfert 1	1630	1030	0.55 ± 0.28	0.64 ± 0.34	219 ± 112
NGC 1068.....	Warm	Seyfert 2	780	320	1.1 ± 0.59	2.0 ± 1.1	42 ± 21
NGC 7479.....	Warm	Seyfert 2	660	410	1.4 ± 0.70	1.6 ± 0.83	13 ± 7

^a References for optical spectral classification: Veilleux et al. (1995) and Ho et al. (1997).

^b In units of L_{\odot} ($\text{K km s}^{-1} \text{ pc}^2$)⁻¹.

^c Star formation rate in $M_{\odot} \text{ yr}^{-1}$.

^d Calculated by adopting $L'_{\text{HCN}}/L'_{\text{CO}} = 0.06$ (see § 5.1).

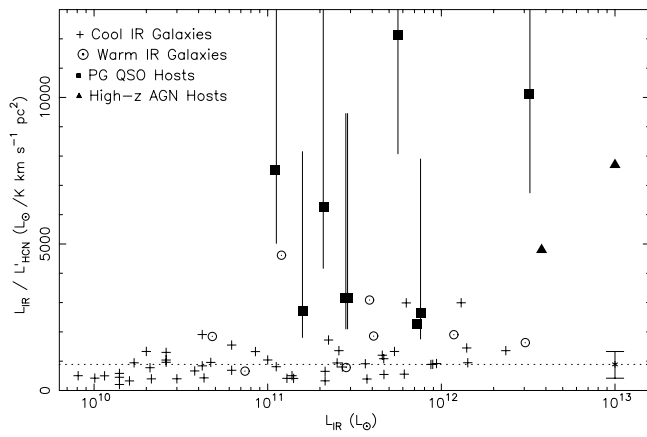


FIG. 7.—Same as Fig. 5, except the estimated $L_{\text{IR}}/L'_{\text{HCN}}$ (see § 5.2) of the PG QSO hosts not detected in HCN are plotted and the y-axis upper limit has been increased. The vertical bars associated with the PG QSO host data points cover the range in $L_{\text{IR}}/L'_{\text{HCN}}$ that results from the uncertainties in eq. (7).

Clearly, a significant fraction of the cool *IRAS* galaxies do harbor AGNs, which may or may not contribute significantly to the heating of dust in their host galaxy. Thus, as a double-check of the results derived from Figure 7, the figure has been replotted with the cool *IRAS* galaxies optically classified as Seyferts and LINER galaxies⁵ omitted (Fig. 8). Galaxies with transitional spectra (e.g., galaxies classified both as LINER galaxies and H II region–like galaxies via different line diagnostics) have been retained, and galaxies with no published classification have also been omitted. Finally, Arp 299, which has an H II region–like optical classification but is known via X-ray observations to harbor an AGN, has been omitted. The main outcome of plotting only the remaining H II region–like galaxies and transitional galaxies is the removal of the outliers in the $L_{\text{IR}}/L'_{\text{HCN}}$ distribution. The value of $\langle L_{\text{IR}}/L'_{\text{HCN}} \rangle_{\text{cool}} (=910 \pm 430)$ remains essentially unchanged.

5.3. Dense Molecular Gas and L_{FIR}

Another obvious issue to consider is whether the above results differ if the far-infrared emission from cool galaxies is considered

⁵ Note that while some of the LINER galaxies are likely primarily starburst galaxies, some of them have strong evidence of embedded AGNs. Thus, the conservative approach of omitting all of the LINER galaxies has been taken for this exercise.

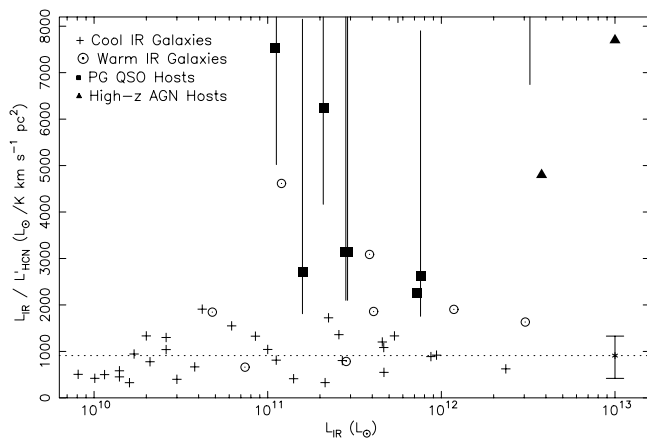


FIG. 8.—Same as Fig. 7, except only the cool *IRAS* galaxies optically classified as H II region–like galaxies or transition galaxies are plotted (Arp 299 has also been omitted; see text). The warm galaxies and PG QSO host data points remain unchanged. Optical emission-line classifications are obtained from Veilleux et al. (1995), Ho et al. (1997), Mazzarella & Boroson (1993), and the NASA/IPAC Extragalactic Database.

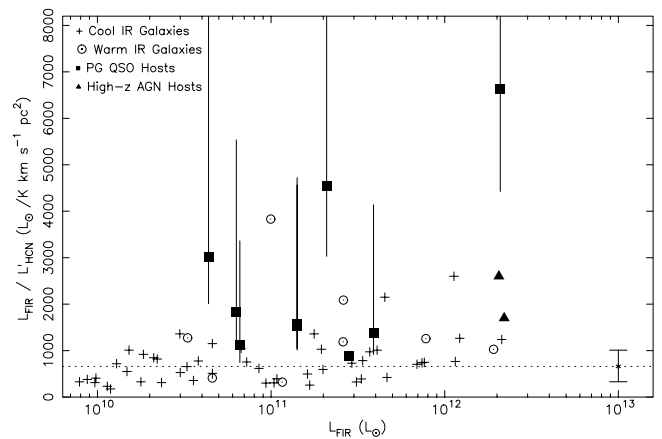


FIG. 9.— $L_{\text{FIR}}/L'_{\text{HCN}}$ vs. L_{FIR} of the PG QSO hosts, a sample of local *IRAS* galaxies, and two high- z AGNs (FSC 10214+4724 and the Cloverleaf Quasar). The dashed line is $L_{\text{FIR}}/L'_{\text{HCN}} = 660 L_{\odot} (\text{K km s}^{-1} \text{pc}^2)^{-1}$ (see § 5.3); the error bar associated with the dashed line encloses 67% (1σ) of the cool galaxy data points.

as the star formation component of the total infrared emission, i.e., if $\langle L_{\text{FIR}}/L'_{\text{HCN}} \rangle_{\text{cool}} \sim L_{\text{SB}}/L'_{\text{HCN}}$. Figure 9 is a plot of $L_{\text{FIR}}/L'_{\text{HCN}}$ versus L_{FIR} of the same samples plotted in Figure 7. The use of L_{FIR} instead of L_{IR} reduces the disparity between the PG QSO and high- z AGN host data points relative to the *IRAS* galaxy data points and shows the possibility that the far-infrared emission in several PG QSO hosts could be due almost entirely to dust heated by young, massive stars (see Table 4). In particular, I Zw 1 has a $L_{\text{FIR}}/L'_{\text{HCN}}$ very near the median value of the cool *IRAS* galaxy population. In the case of the warm galaxies, the median $\langle L_{\text{FIR}}/L'_{\text{HCN}} \rangle_{\text{warm}} (\sim 1220^{+860}_{-810})$ is 33% lower than $\langle L_{\text{IR}}/L'_{\text{HCN}} \rangle_{\text{warm}}$; however, the median value of the cool *IRAS* galaxies, $\langle L_{\text{FIR}}/L'_{\text{HCN}} \rangle_{\text{cool}} \sim 660^{+370}_{-330}$, is 25% lower than $\langle L_{\text{IR}}/L'_{\text{HCN}} \rangle_{\text{cool}}$. Thus, the relative spacing of the warm and cool galaxy data points is only marginally changed by using L_{FIR} . As a result, the contribution of dust heating by young, massive stars to the production of L_{FIR} for the PG QSO hosts and warm galaxies increases by 1%–35% and 1%–12%, respectively, over the contribution derived for L_{IR} (see Table 4). These results reflect the fact that the average $L_{\text{FIR}}/L_{\text{IR}}$ for the cool, warm, and PG QSO galaxies in Figure 8 are 0.77 ± 0.05 , 0.64 ± 0.11 , and 0.44 ± 0.10 , respectively.

5.4. Comparison with Recent Estimates of Star Formation Rates of PG QSO Hosts

The general conclusion that the PG QSO host star formation rates in equation (4) may, in some cases, be overestimates is consistent with a recent study of the star formation rates of QSO hosts by Ho (2005). In this study, star formation rates were derived by first assuming that the $[\text{O II}] \lambda 3727/[\text{O III}] \lambda 5007$ line ratio in QSOs is the same as the constant value measured for the narrow-line regions of Seyfert galaxies, then by attributing excesses in the ratio to star formation within the host. Doing so yields $[\text{O II}] \lambda 3727$ -derived star formation rates of ~ 0.6 – $20 M_{\odot} \text{ yr}^{-1}$; i.e., significantly lower than what would be derived based solely on the assumption that the $L_{\text{IR}} \sim L_{\text{SB}}$ and consistent with the low end of the range in star formation rates estimated for individual hosts in Table 4. Note, however, that the $[\text{O II}] \lambda 3727$ emission line is subject to significant extinction by dust, and thus the Ho (2005) estimates are likely lower limits.

Another study (Schweitzer et al. 2006) addresses the issue of the nature of far-infrared emission in PG QSO hosts by applying the $7.7 \mu\text{m}$ polycyclic aromatic hydrocarbon (PAH)-to-far-infrared luminosity ratio ($L_{\text{PAH}}/L_{\text{FIR}}$) versus $[\text{Ne II}] 12.5 \mu\text{m}$ -to-far-infrared

luminosity ratio ($L_{[\text{Ne II}]} / L_{\text{FIR}}$) diagnostic of starburst galaxies to the QSO host sample. Starburst galaxies are observed to have strong PAH and weak $[\text{Ne II}]$ relative to AGN-dominated hosts because the AGN efficiently destroys PAHs and is able to produce extended semi-ionized regions in which neon is collisionally excited. Schweitzer et al. concluded that 30% or more of the far-infrared emission is due to dust heating by young, massive stars. By comparison, a median percentage of $42^{+56}_{-35}\%$ is estimated from the present analysis of the HCN data.

5.5. The Effects of the AGN on HCN Emission

Throughout this paper the assumption has been made that HCN is collisionally excited by molecular hydrogen. Recent papers have challenged this claim by stating that in galaxies harboring AGNs, X-ray emission from the AGN enhances HCN emission (e.g., Kohno et al. 2003; Gracia-Carpio et al. 2006). The high $L_{\text{IR}} / L'_{\text{HCN}}$, and thus the low L'_{HCN} , of most of the PG QSO hosts, high- z AGN hosts, and warm galaxies relative to cool *IRAS* galaxies (Fig. 7) clearly contradict this hypothesis.

To examine this issue another way, consider again the plot of $L'_{\text{HCN}} / L'_{\text{CO}}$ versus L_{IR} of the QSO hosts and *IRAS* galaxies (Fig. 6). In this figure I Zw 1 and most of the Seyfert galaxies have $L'_{\text{HCN}} / L'_{\text{CO}} < 0.1$, consistent with the distribution of the H II region-like galaxies. Two of the Seyfert galaxies have $L'_{\text{HCN}} / L'_{\text{CO}} > 0.1$; however, they are still within the distribution of $L'_{\text{HCN}} / L'_{\text{CO}}$ of H II region-like and LINER galaxies. Thus, there is no evidence that the global HCN emission is enhanced relative to CO by the presence of a powerful AGN.

6. CONCLUSIONS

New CO and HCN observations of a sample of $z < 0.17$ optically selected PG QSO hosts with infrared excesses are presented. These data have been compared with similar data of *IRAS*-detected galaxies to assess the validity of using the infrared luminosity to estimate star formation rates in luminous AGN hosts. The following conclusions are reached:

1. The new CO measurements confirm the results presented in Evans et al. (2001), that QSO hosts as a class may have low values of L'_{CO} for their L_{IR} relative to *IRAS* galaxies, or relatively high values of $L_{\text{IR}} / L'_{\text{CO}}$. Such high $L_{\text{IR}} / L'_{\text{CO}}$ ratios may be evidence that AGNs contribute significantly to the heating of dust in their host galaxies, or that they have high star formation efficiencies.
2. A comparison of the QSO hosts and *IRAS* galaxies surveyed in HCN(1 \rightarrow 0) to date show the upper distribution of $L_{\text{IR}} / L'_{\text{HCN}}$ (> 1600) to be mostly populated by warm *IRAS* galaxies and AGN hosts. This distribution overlaps at the low end with cool *IRAS* galaxies for which $\langle L_{\text{IR}} / L'_{\text{HCN}} \rangle_{\text{cool}} \sim 890^{+440}_{-470} L_{\odot}$ ($\text{K km s}^{-1} \text{pc}^2$) $^{-1}$. There are also two (out of eight) warm galaxies with $L_{\text{IR}} / L'_{\text{HCN}}$ comparable to the median $L_{\text{IR}} / L'_{\text{HCN}}$ of cool

galaxies. An enhanced $L_{\text{IR}} / L'_{\text{HCN}}$ relative to cool *IRAS* galaxies thus appears to be an indication that an AGN is contributing significantly to heating the dust. However, the possibility that the dust in most of the QSO hosts and warm galaxies is heated primarily by young, massive stars cannot be entirely ruled out. If the median ratio of $L'_{\text{HCN}} / L'_{\text{CO}} \sim 0.06$ observed for Seyfert galaxies and the PG QSO host I Zw 1 is applied to the PG QSOs not detected in HCN, then the derived $L_{\text{IR}} / L'_{\text{HCN}}$ ratios correspond to a stellar contribution to the production of L_{IR} of $\sim 7\% - 35\%$ and star formation rates of $\sim 2 - 37 M_{\odot} \text{yr}^{-1}$ are derived for the QSO hosts. The corresponding values for the warm galaxies are $\sim 10\% - 100\%$ and $\sim 3 - 220 M_{\odot} \text{yr}^{-1}$.

3. The average $\langle L_{\text{FIR}} / L_{\text{IR}} \rangle$ of the cool, warm, and PG QSO galaxies considered in this study is 0.77 ± 0.05 , 0.64 ± 0.11 , and 0.44 ± 0.10 , respectively. Thus, the disparity between the QSO (and high-redshift AGN) hosts and the cool galaxies is diminished by comparing the L_{FIR} of QSO hosts and cool galaxies. If the far-infrared is adopted as the star formation component of the total infrared in cool galaxies, i.e., $\langle L_{\text{FIR}} / L'_{\text{HCN}} \rangle_{\text{cool}} \sim L_{\text{SB}} / L'_{\text{HCN}}$, then five of the nine QSO hosts, including I Zw 1, potentially have all of their L_{FIR} generated by dust heated by massive stars. The stellar contributions to L_{FIR} in QSO hosts are up to 35% higher than those derived for L_{IR} , but the warm galaxies have contributions only 10% higher than those derived for L_{IR} .

4. The PG QSO host I Zw 1 and the *IRAS* galaxies with Seyfert optical classifications have $L'_{\text{HCN}} / L'_{\text{CO}}$ distributions comparable to H II region-like galaxies. It is thus unlikely that the global HCN emission in galaxies harboring luminous AGNs is enhanced relative to CO by radiation from the AGN.

An HCN survey of a more statistically complete sample of *IRAS* galaxies and PG QSO hosts is required to assess the robustness of many of these results. The apparent faintness of HCN emission in PG QSO hosts, and in many warm galaxies, necessitates the use of a larger millimeter-wave telescope. Such observations may be possible with the soon-to-be commissioned 50 m diameter Large Millimeter Telescope or the 100 m diameter Green Bank Telescope (GBT). Frequencies as high as 90 GHz should be accessible with the GBT in a few years.

We thank the telescope operators and staff of the IRAM 30 m telescope for their support both during and after the observations and the anonymous referee for critical comments that greatly improved the accuracy and clarity of the paper. A. S. E. also thanks J. Mazzarella, T. Bertram, and J. Mulchaey for useful discussions and assistance. A. S. E. was supported by NSF grant AST 02-06262. This research has made use of the NASA/IPAC Extragalactic Database, which is operated by the Jet Propulsion Laboratory, California Institute of Technology, under contract with the National Aeronautics and Space Administration.

REFERENCES

- Alloin, D., Barvainis, R., Gordon, M. A., & Antonucci, R. R. J. 1992, *A&A*, 265, 429
- Barvainis, R., Alloin, D., & Antonucci, R. 1989, *ApJ*, 337, L69
- Della Ceca, R., et al. 2002, *ApJ*, 581, L9
- Elitzur, M., Nenkova, M., & Ivezić, Z. 2004, in *ASP Conf. Ser. 320, The Neutral ISM in Starburst Galaxies*, ed. S. Aalto, S. Huettemeister, & A. Pedlar (San Francisco: ASP), 242
- Evans, A. S. 2003, in *ASP Conf. Ser. 320, The Neutral ISM in Starburst Galaxies*, ed. S. Aalto, S. Huettemeister, & A. Pedlar (San Francisco: ASP), 222
- . 2006a, in *Extreme Starbursts, Near and Far*, ed. Y. Gao & D. Sanders (Publ. Purple Mountain Obs.), in press
- . 2006b, *NewA Rev.*, in press
- Evans, A. S., Frayer, D. T., Surace, J. A., & Sanders, D. B. 2001, *AJ*, 121, 3285
- Evans, A. S., Mazzarella, J. M., Surace, J. A., Frayer, D. T., Iwasawa, I., & Sanders, D. B. 2005, *ApJS*, 159, 197
- Gao, Y., & Solomon, P. M. 2004a, *ApJS*, 152, 63
- . 2004b, *ApJ*, 606, 271
- Gracia-Carpio, J., Garcia-Burillo, S., Planesas, P., & Colina, L. 2006, *ApJ*, 640, L135
- Guyon, O., Sanders, D. B., & Stockton, A. 2006, *ApJS*, 166, 89
- Haas, M., et al. 2003, *A&A*, 402, 87
- Ho, L. 2005, *ApJ*, 629, 680
- Ho, L., Filippenko, A. V., & Sargent, W. L. 1997, *ApJS*, 112, 315
- Imanishi, M., Nakanishi, K., & Kohno, K. 2006, *AJ*, 131, 2888
- Imanishi, M., Nakanishi, K., Kuno, N., & Kohno, K. 2004, *AJ*, 128, 2037

- Kennicutt, R. C., Jr. 1998, *ARA&A*, 36, 189
- Kohno, K., Ishizuki, S., Matsushita, S., Vila-Vilaro, B., & Kawabe, R. 2003, *PASJ*, 55, L1
- Mazzarella, J. M., & Boroson, T. A. 1993, *ApJS*, 85, 27
- Mazzarella, J. M., Graham, J. R., Sanders, D. B., & Djorgovski, S. 1993, *ApJ*, 409, 170
- Sanders, D. B., Mazzarella, J. M., Kim, D. C., Surace, J. A., & Soifer, B. T. 2003, *AJ*, 126, 1607
- Sanders, D. B., & Mirabel, I. F. 1996, *ARA&A*, 34, 749
- Sanders, D. B., Phinney, E. S., Neugebauer, G., Soifer, B. T., & Matthews, K. 1989, *ApJ*, 347, 29
- Sanders, D. B., Scoville, N. Z., & Soifer, B. T. 1988a, *ApJ*, 335, L1
- Sanders, D. B., Soifer, B. T., Elias, J. H., Madore, B. F., Matthews, K., Neugebauer, G., & Scoville, N. Z. 1988b, *ApJ*, 325, 74
- Sanders, D. B., Soifer, B. T., Elias, J. H., Neugebauer, G., & Matthews, K. 1988c, *ApJ*, 328, L35
- Schmidt, M., & Green, R. F. 1983, *ApJ*, 269, 352
- Schweitzer, M., et al. 2006, *ApJ*, 649, 79
- Scoville, N. Z., Frayer, D. T., Schinnerer, E., & Christopher, M. 2003, *ApJ*, 585, L105
- Solomon, P. M., Downes, D., Radford, S. J. E., & Barrett, J. W. 1997, *ApJ*, 478, 144
- Solomon, P. M., Vanden Bout, P. A., Carilli, C., & Guelin, M. 2003, *Nature*, 426, 636
- Stockton, A., & MacKenty, J. W. 1983, *Nature*, 305, 678
- Surace, J. A., Sanders, D. B., & Evans, A. S. 2001, *AJ*, 122, 2791
- Vanden Bout, P. A., Solomon, P. M., & Maddalena, R. J. 2004, *ApJ*, 614, L97
- Veilleux, S., Kim, D.-C., Sanders, D. B., Mazzarella, J. M., & Soifer, B. T. 1995, *ApJS*, 98, 171
- Veilleux, S., et al. 2006, *ApJ*, 643, 707
- Xia, X. Y., Xue, S. J., Mao, S., Boller, Th., Deng, Z. G., & Wu, H. 2002, *ApJ*, 564, 196
- Zezas, A., Ward, M. J., & Murray, S. S. 2003, *ApJ*, 594, L31